Meissner holes and turbulent structures in superconductors in unidirectional and rotating fields

V. K. Vlasko-Vlasov
Institute of Solid State Physics RAS, 142432 Chernogolovka, Russia
and Argonne National Laboratory, 9700 South Cass Ave., Argonne, Illinois 60439

U. Welp, G. W. Crabtree, and D. Gunter
Argonne National Laboratory, 9700 South Cass Ave., Argonne, Illinois 60439

V. V. Kabanov and V. I. Nikitenko
Institute of Solid State Physics RAS, 142432 Chernogolovka, Russia

L. M. Paulius
Western Michigan University, Kalamazoo, Michigan 49008
(Received 27 October 1997)

Flux distributions on different faces of YBCO crystal plates remagnetized by unidirectional and rotating fields are studied using advanced magneto-optical techniques. Bending of vortex lines is shown to be crucial for the remagnetization process even in plates with large width to thickness ratios in in-plane fields. Closed vortex loops smaller than a critical radius collapse, forming a flux-free cylinder: the Meissner hole. This results in the collection of superconducting currents into cords along the Meissner holes and the formation of turbulent flux patterns. Similar structures and unusual patterns are found when the field is rotated in the basal or end face plane. Values of the currents in the structures are retrieved from fits of measured flux profiles by model current distributions. The remagnetization patterns revealed in rotating fields are important for understanding the behavior of superconducting parts in motors and levitating devices. [S0163-1829(98)08929-2]

I. INTRODUCTION

It was shown recently that upon remagnetization of YBCO crystal plates in perpendicular magnetic fields, characteristic flux and current structures associated with strong bending of flux lines are formed.[1] Remagnetization of these samples proceeds not due to motion of a flat boundary between straight oppositely polarized vortices, as visualized in the Bean model for infinite slabs, but due to compression and expansion of induction loops. In any finite sample induction lines must close in order to satisfy the Maxwell equation $\mathrm{div}\, B=0$. These loops are easy to visualize in the case of trapped flux in normally magnetized plates. As shown in Fig. 1, the induction lines close near the edges of the plate around lines that are defined by the condition $B=0$. When the field is parallel to the plate, the curvature of induction lines is usually ignored. It turns out, however, that this simplification ignores some important effects appearing in real samples.

Inside a superconductor, closed vortex loops tend to shrink due to their line tension,[2] as expected for any elastic string. This shrinkage is opposed by pinning forces, which tend to immobilize the vortices. As was shown by Koppe[3] and Evetts and Campbell,[2,4] vortex loops of radii below a critical value $R_c=\sigma/F_p$, determined by the equilibrium between the line tension σ and the pinning force F_p, will collapse. Inside the critical radius there is a flux-free cylinder, the Meissner hole (see Fig. 1). In an increasing remagnetizing field this structure moves to the interior of the sample by asymmetric collapse of the inner vortex loops. In the λ layer along the surface of the cylinder, a strong magnetization current J_M flows that can modify neighboring field distributions. It is associated with the local change of B from zero inside the Meissner hole to $\sim B_{c1}$ in the surrounding vortex phase. The current and field are related through Maxwell's equation $\mathrm{rot}\, B=\mu_0 J$, which may be simplified to $J_M \sim B_{c1}/\mu_0\lambda$. The large magnetization current and field gradient at the boundary between the vortex and Meissner phases is often called the dB/dH effect and has been extensively discussed.[2,5–10]

In the present work, features of Meissner holes in various experimental geometries have been investigated using magneto-optical imaging. It is shown that at any orientation of the field with respect to the sample the remagnetization proceeds generally due to bending of flux lines. Even in the case of thin plates in parallel fields, these effects turn out to

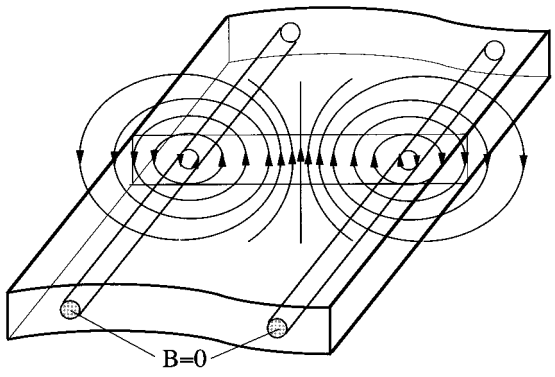

FIG. 1. Scheme of magnetic flux lines due to trapped flux in a superconducting plate magnetized by a normal field. Two flux-free cylinders where $B=0$ are the Meissner holes as described in the text.

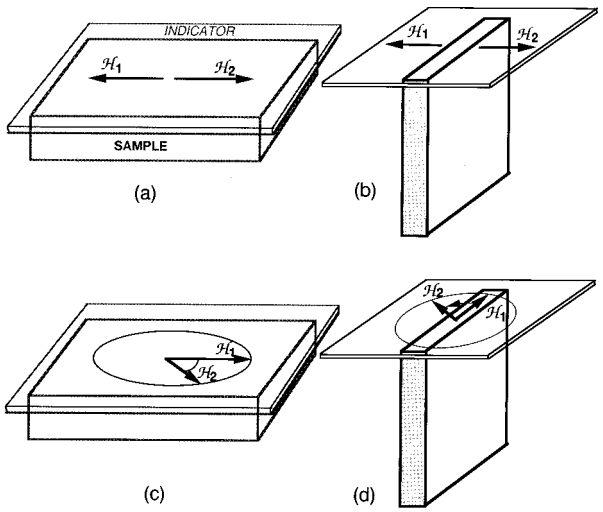

FIG. 2. The applied fields and sample orientations studied in this work. The optical axis of the microscope is vertical.

be crucial. They result in the formation of complex current and field patterns with widely variable local density and direction (see also Ref. 11). An especially rich variety of unusual current and induction structures due to flux bending is found in rotating fields.[12] Their nucleation and evolution are important in the operation of rotors, bearings, and other moving parts made of superconductors.

This paper is organized as follows. In Sec. II, details of the experimental technique and the investigated samples are given. In Sec. III the remagnetization behavior in fields of various orientations is discussed for fields applied parallel to the wide face of the platelike sample (Sec. III A), and for fields normal to this face (Sec. III B). In Sec. IV the remagnetization behavior for rotating in-plane fields is presented. In Sec. IV A the qualitative features are analyzed whereas in Sec. IV B a detailed quantitative description of the remagnetization front for isotropic as well as for anisotropic superconductors is given. It is shown that in anisotropic superconductors the critical currents outside the Meissner cylinder give the dominant contribution to the observed field patterns. Section V presents the effect of field rotation in the narrow end faces of the samples.

II. EXPERIMENTAL

YBCO single crystals with different aspect ratios (width/thickness in the range of 5–40) were placed on the cold finger of a cryostat and covered with an iron garnet magneto-optical indicator film (for details see Ref. 13). Observations of induction patterns using a polarizing microscope were made with the fields parallel to the imaged planes of the samples (i.e., fields were perpendicular to the optic axis of the microscope). Flux images on the wide ab surfaces and narrow ac/bc faces were studied. In the latter case, the samples were mounted with their narrow face perpendicular to the light axis. The relevant geometries and field orientations are shown in Fig. 2.

Magneto-optical observations based on the Faraday effect detect only the field component normal to the imaged plane of a sample B_n. Thus the magneto-optical images reveal tilts of the induction from the direction of the external field. Using calibration curves, which represent the average intensity in the indicator film without a sample as a function of the normal field, the magneto-optical images were transformed into maps of B_n on the sample surfaces. From these maps it was possible to recover qualitative pictures of current structures in the plates. Quantitative estimates of currents were obtained using a numerical fitting of $B_n(x)$ scans along a chosen line by model current configurations. Although the recovery of three-dimensional current distributions from two-dimensional induction pictures is not unique, the use of physically reasonable models allows important features to be determined.

We start with observations of remagnetization patterns in a unidirectional field parallel to the wide ab planes of the samples as illustrated in Fig. 2(a). These patterns are compared with previous results with the field along the c axis, normal to the plates, as shown in Fig. 2(b). We then introduce and discuss more complicated structures that occur as the field is rotated in the ab [Fig. 2(c)] and ac/bc [Fig. 2(d)] faces and relate many of their features to patterns found in unidirectional fields. Finally, a model of Meissner holes in anisotropic superconductors with enhanced critical currents around flux-free cylinders that fit induction profiles observed in all experimental geometries is discussed.

III. UNIDIRECTIONAL REMAGNETIZATION

A. Parallel fields

Remagnetization of plates in parallel fields is usually considered to be homogeneous in the planes parallel to the surface. However, even in strong in-plane fields, edge effects turn out to be essential. They create normal induction components everywhere on the surface of the sample, even in the center of large faces parallel to the external field.

The main features observed in the magnetization process of a zero-field-cooled plate in parallel field are shown in Fig. 3. Sample dimensions and applied fields are presented in the figure captions. The images are taken at 40 K. On initial application of the field, a bright area appears on the right edge and a dark area on the left edge, corresponding to positive and negative components of the normal field as shown in Fig. 3(a). Such a curvature of the field lines is due to the partial screening of the field by the superconductor as illustrated in Fig. 4(a). This screening has two origins: surface currents due to the Meissner effect and the Bean-Livingston barrier, and bulk critical currents that arise from pinning. The surface currents give rise to a sharp drop in the normal field just inside the sample, and are responsible for the clear outline of the sample in Fig. 3. The bulk currents produce a slow variation of the normal field that persists to the center of the sample. In Fig. 3(a) there is a distinct irregular sawtooth or zigzag boundary that divides the sample image into a bright region on the right and a dark region on the left. These regions define opposite directions of the normal field on the sample surface. The sharpness of the boundary is remarkable. It shows that the normal field changes sign discontinuously. Such an effect may be expected from the boundary condition on the vortex currents, which near the surface can have no normal component. The local field of vortices must therefore be normal and cannot be zero as long

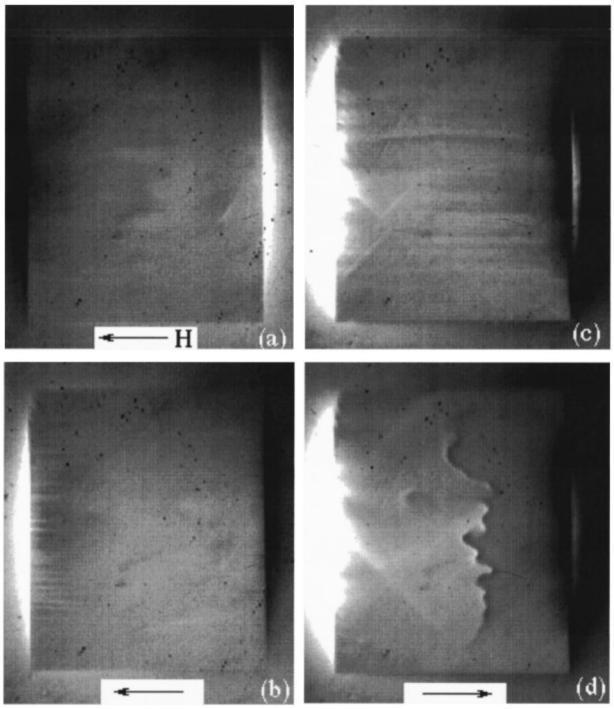

FIG. 3. Formation of the Meissner hole during the in-plane remagnetization of a $780\times650\times150\ \mu$m YBCO crystal at $T=40$ K. (a) $H=1235$ Oe applied after zero-field cooling the sample, (b) $H=1235$ Oe decreased from 1800 Oe, (c) remnant state after reducing H to zero from (b), (d) $H=-320$ Oe after (c).

as vortices are present. Calculations of the equilibrium shape of inclined vortices near the surface of a superconductor[14] confirm this conclusion.

With decreasing field the contrast at the edges becomes reversed as illustrated in Fig. 3(b) and bright stripes (on the left and on the right) along the field direction appear. In these stripes near the edges, the normal component of the field reverses, compared to the increasing field case of Fig. 3(a). This corresponds to upward bending of the vortices at the edges as illustrated in Fig. 4(b), in contrast to downward bending as in Fig. 4(a). The flux image of the sample in the remnant state after the field has been reduced to zero is shown in Fig. 3(c). The image is qualitatively similar to Fig. 3(a), except that the bright and dark regions are inverted, indicating that the curvature of the field lines is opposite. Also, the zigzags of the sawtooth boundary are much longer than in the high field. Calculated field lines representing the remnant state are shown in Fig. 4(d), based on the current distribution in Fig. 4(c).

The application of a small reverse field produces the image illustrated in Fig. 3(d). A feature appears near the center of the sample at the boundary between regions of small opposite normal field, where an additional sharp contrast has developed. This contrast indicates a locally high normal field that changes sign at the boundary. This is similar to the field pattern around a current carrying wire, and implies a substantial current flowing along the boundary. A similar concentration of the field at the boundary between oppositely magnetized regions was observed in the case of a normally magnetized plate.[1,11] This structure is the signature of the Meissner hole. The increased current along the Meissner

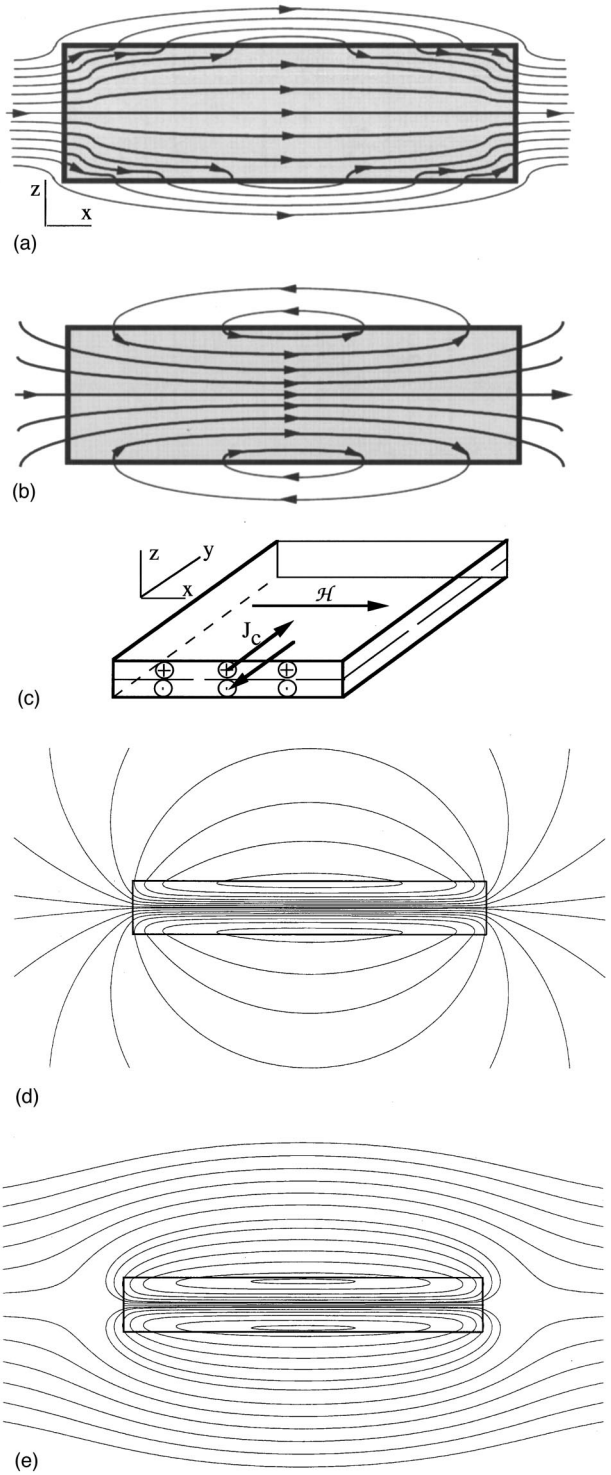

FIG. 4. Curvature of flux lines after application (a) and decrease (b) of an in-plane field. (c) current distribution and applied field for the calculated field lines shown in (d) and (e). (d) field lines for the remnant state ($H=0$), (e) field lines for the beginning of remagnetization obtained by adding to (d) a small negative field $H=-0.008$ (in units of $J_c\Delta$, where Δ is the plate thickness).

hole results in its bending instability, as discussed in Ref. 1. It is similar to the pinch effect; an instability of an electrical current in a plasma discharge in a magnetic field.[15] In Fig. 3(d) the bending of the Meissner hole is pronounced. With further increasing field the image of the Meissner hole dis-

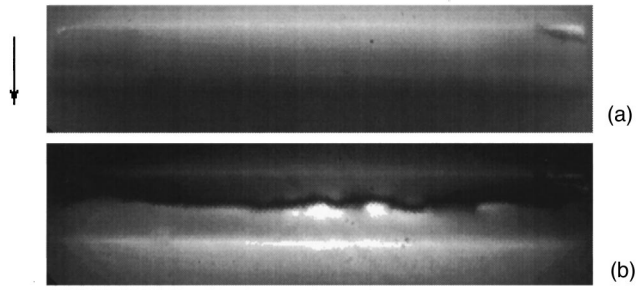

FIG. 5. Formation of the Meissner hole on the end face during remagnetization of the plate in the perpendicular field. The field of 1890 G along the vertical direction is applied (a) and decreased to 0 (b) at 50 K. The Meissner hole is revealed as a wiggling horizontal dark line with brighter edges in the middle of the sample in (b).

appears. The disappearance is associated with the motion of the Meissner hole down toward the middle plane of the plate where it annihilates with a second Meissner hole of opposite chirality moving up from the bottom surface of the sample. Figure 4(e) shows calculated field lines in an infinite bar with the same cross section as the sample in Fig. 3 that has been remagnetized by a small negative field. Closed field loops centered on positions where $B=0$ near the top and bottom surfaces indicate the regions where Meissner holes will form.

This picture of the Meissner hole shrinking in the plane perpendicular to the field like a belt tightening around the sample during remagnetization is quite different from the commonly accepted scenario of motion of a flat front parallel to the faces of a plate, as envisioned in the Bean model. In the latter case, this front should carry a large Meissner current $[\sim 2(B_{c1}/\lambda)\lambda D$, where D is a typical in-plane dimension of the sample] that would give a substantial contribution ΔM_m to the magnetization of the sample. From our picture it follows that ΔM_m is determined by the currents in the Meissner hole that are smaller by a factor $\sim R_c/D$ than those in the flat front picture. The absence of the ΔM_m contribution in Nb ribbons in parallel fields, reported recently by LeBlanc *et al.*,[9] is consistent with our model of bending vortices.

B. Perpendicular field

The above results for the parallel geometry show a remarkable similarity with those observed earlier[1] for a thin plate in a perpendicular field. The experiment is illustrated by Fig. 2(b). In Ref. 1 Meissner holes were shown to nucleate in the middle of the narrow end faces along the perimeter of the plate, and to move to the center of the sample with increasing remagnetizing field. The appearance of the Meissner hole on the end face is shown in Fig. 5. The Meissner hole is visible in Fig. 5(b) as a black line near the center of the face surrounded by brighter regions. (In this picture, the polarizers in the microscope have been adjusted so that zero normal field is black and positive and negative fields of the same magnitude are only slightly unequal in intensity.) The Meissner hole is wiggling both in the plane of observation and perpendicular to it. Variations in intensity along the Meissner hole are associated with variations in depth of the Meissner hole from the sample surface.

The nucleation of the Meissner hole on reducing the field from its maximum value is described by the field line distribution shown in Fig. 6. In this case the critical state was modeled by currents of a constant density flowing perpendicular to the plane of the picture in opposite directions in the top and bottom halves of the plate, as illustrated in the inset. The fields of these currents are superimposed on the constant external field. At some value of the latter, the center of the closed field loops (where $B=0$) near the edges, as shown in Fig. 6, and here the Meissner hole is formed. As the external field is decreased and changes polarity, the structure moves inside the sample.

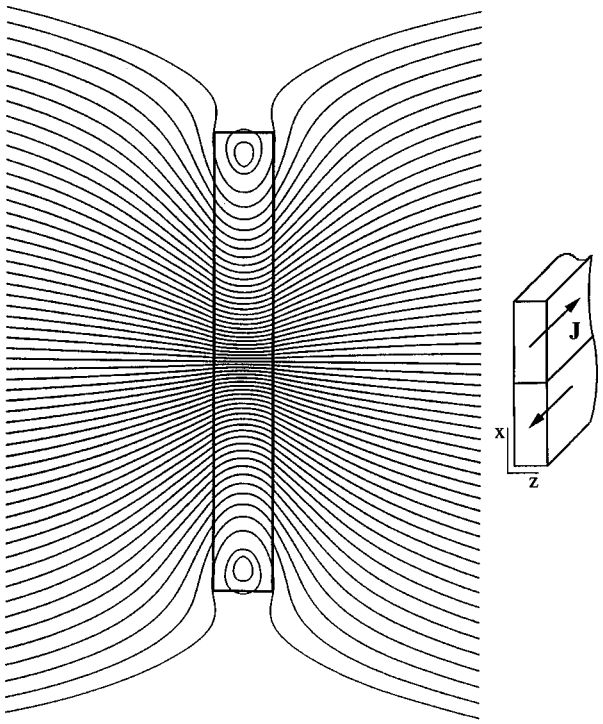

FIG. 6. Calculated field lines in an infinite plate with the same cross section as that of the sample in Fig. 5 with currents flowing as shown in the inset. The closed field lines near the ends of the plate indicate the location of the Meissner holes formed at reduction of the external field.

It is easy to see that experimental pictures and field line patterns for parallel (Figs. 3 and 4) and perpendicular (Figs. 5 and 6) geometries are topologically identical. They can be transformed one into another by scaling along appropriate axes.

IV. ROTATION OF IN-PLANE FIELDS

A. Qualitative discussion of flux images

The main features of the induction patterns in the rotated ab fields are illustrated by Fig. 7 for a rectangular sample containing only a few twin boundaries. The sample was zero-field cooled and then a field was applied parallel to its width and rotated clockwise. The field direction is indicated by an arrow in each picture. In Fig. 7(a), taken in the horizontal field $H_{\rm ext}=970$ Oe at $T=40$ K, a strong increase of the magnitude of the normal field near the edges and a sawtooth boundary separating areas of opposite normal fields, are observed, as discussed earlier in connection with Fig. 3.

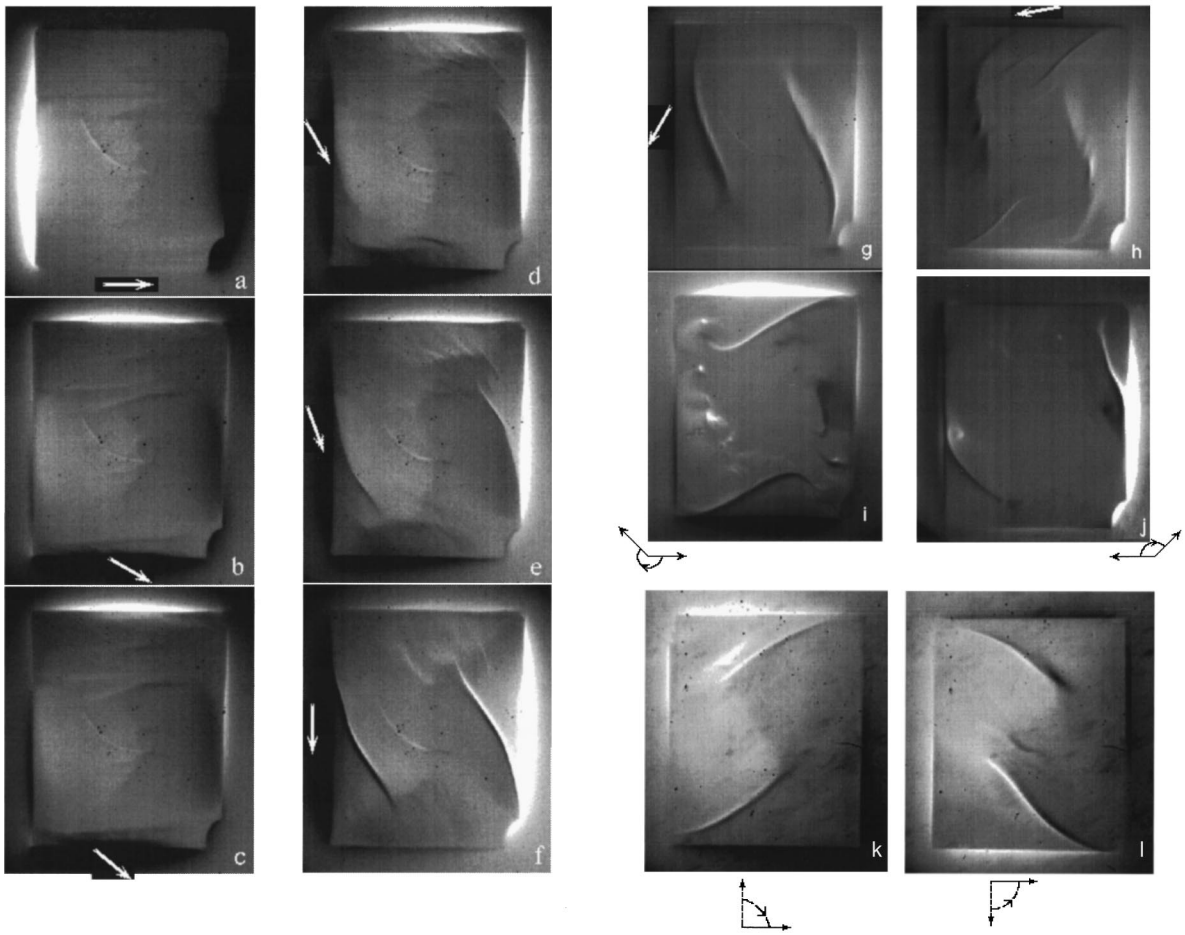

FIG. 7. (a)–(f) Changes of the flux distribution on the ab surface of a $760\times625\times110$ μm YBCO single crystal due to in-plane field rotation at $T=40$ K. $H=960$ G is applied to the sample after zero-field cooling along the horizontal axis and rotated clockwise as shown by arrows. Bright and dark intensity corresponds to up and down fields normal to the ab plane. (i) shows a flux pattern after rotation of H by $2\pi+240°$. In (j) the field of 1880 G along the horizontal axis was switched on and off at 30 K, then an opposite field $H=-650$ G was applied and turned by 130° cw. In (k) and (l) the field $H=500$ G was applied to the zero-field-cooled sample at 55 K and turned by $\sim 90°$ cw and ccw, respectively, as shown in the sketch.

Upon rotation of the external field in the ab plane, a bright intensity, indicating the normal field strength, develops at the horizontal x edges and decreases at the vertical y edges. This effect increases with increasing rotation angle α. At $\alpha>20°$, bright bands appear very near the top and bottom edges of the sample, as shown in Fig. 7(b) (here $\alpha=30°$). At larger angles a changing modulated structure of brighter and darker stripes develops in these bands [Figs. 7(c) and 7(d)]. These structures correspond to up and down declinations of vortices from the ab plane that can be associated with helical perturbations of the flux structure.[16,17] When H turns from the initial x direction in Fig. 7(a) its y component increases. The y component of the rotated field induces vortices tilted up and down from the ab plane near the top and bottom x edge of the sample, where formerly the trapped field was predominantly in the ab plane. New vortices cut and reconnect with the trapped ones,[2,18,17] thus forming flux lines with normal components that produce the bright and dark intensities. Under these conditions, the currents along x, induced by the y component of the field, can cause a helical instability of x-oriented vortices.[16,17] This can produce the modulation of B_n at the surface, as occurs near the x edges of the sample in Figs. 7(c)–7(e). The details of the helical instabilities in rotating fields can be treated in the framework of the Brandt[17] and Clem and Perez-Gonzales[19] theories. Here we give only an estimation of the pitch of the helices L_h. Following Brandt,[17] $L_h\sim 4.4[\alpha_L/c_{11}]^{-1/2}$ where $\alpha_L\sim J_cB/(\Phi_0/B)^{1/2}$ is the Labush parameter (pinning force/intervortex distance) and $c_{11}\sim B^2/\mu_0$. For $B=1000$ G and the critical current $J_c\sim 10^5$ A/cm^2 [the value of J_c is taken from fits of the measured $B_n(x)$ profile in Fig. 10(a)], one gets $L_h\sim 15$ μm. This estimate is in reasonable agreement with the experimental period of the modulated pattern near the horizontal edges in Fig. 7(c). Similar modulations appear at the vertical edges when the field passes through the vertical direction. Note that L_h is proportional to $(B)^{1/4}$ and $(J_c)^{-1/2}$, so the estimate will not change much with these parameters.

At angles of about 30°, the contrast at the y edges starts inverting [Fig. 7(b)]. Vortices that were trapped here by the initial application of the field with their ends tilted down [towards the middle ab plane of the sample, Fig. 8(a)] now change their configuration to accommodate the rotated external field. The reduced field in the original direction allows vortices in the corners to exit from the sample. The remaining vortices here become concave upward, as shown in Fig.

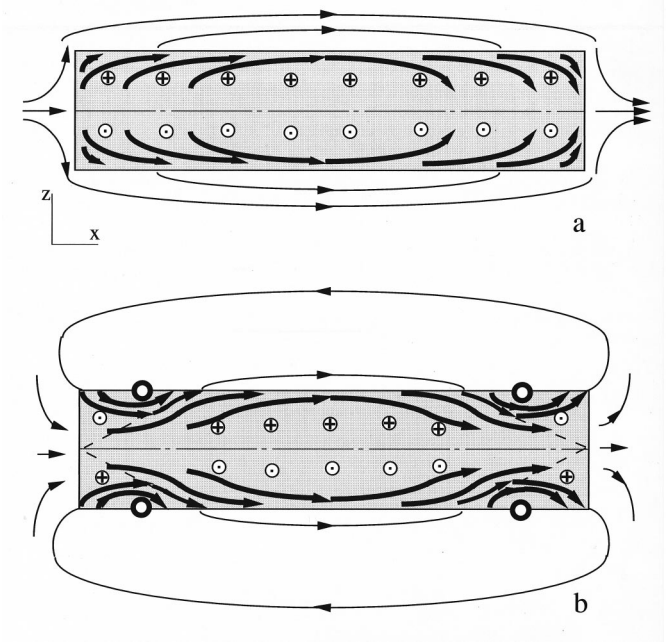

FIG. 8. Bending of flux lines in the central cross section of a plate after the application of the field [(a) as in Fig. 7(a)] and after turning the field by 90° [(b) as in Fig. 7(f)]. In the regions shown by thick circles vortices close into loops and form Meissner holes. Circles with crosses and points show opposite current directions.

8(b). This process is inhomogeneous along the sample edges. One can see in Fig. 7(b) bright and dark regions on both left and right edges of the crystal. Such an inhomogeneity is determined by the rectangular shape of the sample. It corresponds to a concave upward tilt of field lines in regions of inverted contrast and a concave downward tilt where the contrast did not change. The above picture can be associated with currents flowing in opposite directions along bright and dark parts of the edge and meeting at the points where the normal field changes sign.

The sawtooth boundary between slightly brighter and darker halves of the sample also changes as the field rotates. It assumes an *S*-like shape with its ends as marked by small arrows in Fig. 7(d). Variations of the boundary from its initial shape directly outline the area where vortices have inverted their curvature in response to the reduced x and increased y components of the applied field. These changes take place more obviously at the periphery of the sample, while in the middle area the flux remains mainly unchanged. The spatial division of the sample into areas where the flux adapts to the rotated field orientation or remains trapped in the original direction is consistent with magnetization measurements by Hasan and Kouvel (Ref. 20 and references therein). They found two components of the magnetization of polycrystalline YBCO disks rotated in an external field parallel to the plane of the disk. One component remained locked to the sample, as we observe near the middle of our crystal, and one followed the field direction with a lag of several degrees. Earlier magnetization measurements of low-T_c discs in rotating fields by Boyer and LeBlanc[21] were also explained by the presence of evolving and unchanging flux regions. However, they were suggested to be outer and inner layers parallel to the disk surface, respectively. Our measurements show that the evolving component of the flux arises in the edge regions of the sample.

The most remarkable features develop at the ends of the *S* boundary near the y edges when the field turns by more than $\sim 50°$ [Figs. 7(d) and 7(e)]. Here the boundary starts transforming into lines with substantially higher contrast, bright on one side and dark on the other. With further field rotation this contrast increases more. Bright lines stretch inside the sample and towards the edges [Fig. 7(f)]. Note that the lines develop when the contrast at the y edges is reversed with respect to the initial state in Fig. 7(a). The corresponding inversion of the curvature of vortices at the edge is shown in Fig. 8(b) that illustrates the vortex shape in the central xz cross section of the sample after rotation of H from the x axis in Fig. 8(a) to the y axis ($\alpha \sim 90°$). It corresponds to the inversion of the current direction in the corners roughly outlined by dashed lines just where vortices change their curvature.

The observed strong bright and dark intensities mark the formation of Meissner holes in the rotated field geometry. As in unidirectional remagnetization illustrated by Fig. 3(d), the concentration of up and down flux on either side of the Meissner hole implies a substantial local current flowing along its length.

With further field rotation ($\alpha > 90°$), the Meissner holes turn, following the field direction with a lag angle. Then the structure becomes unstable, similar to the pinched plasma that shows kink instabilities.[15] Images of the lines become wider and decay into parts that shift with respect to each other [Figs. 7(g)–7(h)]. Strong current lines appear near the x edges when the field is turned by more than 140° [Fig. 7(h)], in the same way as they developed at the y edges for smaller rotation angles.

Current pinches continuously nucleate and decay as the field rotates beyond $\sim 140°$ and finally a rather complicated flux structure is formed [Fig. 7(i), $\alpha = 2\pi + 240°$]. As the Meissner holes decay, their ends sometimes form spirals with bright spots in the foci [Fig. 7(j)]. Also, parts of the lines transform into round shaped bundles of perpendicularly magnetized vortices and move into the bulk [such bright and dark spots can be seen in Figs. 7(i) and 7(j)]. These detached macroscopic flux bundles or macroturbulent structures are nucleated, due to the bending instability and decay of the current pinches similar to the case of plates in a perpendicular field where flux bundles appear at the front between up and down magnetized regions.[11,1]

Using the field distributions for straight and curved current lines and for current carrying tapes, it is possible to build a qualitative picture of currents corresponding to the observed flux images. Such schemes of currents near the surface of the sample reproducing the main features observed in Figs. 7(i) and 7(j) are shown in Figs. 9(a) and 9(b), respectively. Here stronger local currents are shown by thicker lines. The directions and curvature of the current lines give the proper variations in the magnitude and direction of B_n, in accordance with the observed flux patterns. Currents in the central area are associated with the initial field application. This is illustrated by the observation that the flux and thus the current distribution does not change so strongly in the center as at the periphery of the sample.

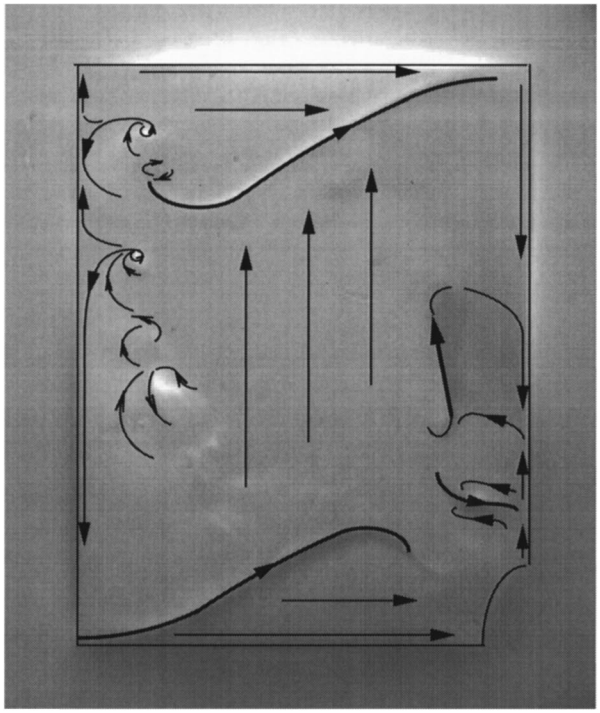

(a)

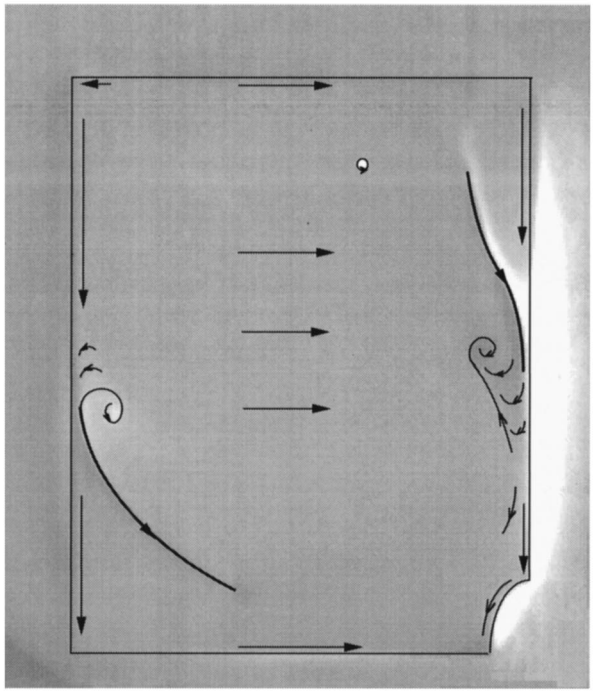

(b)

FIG. 9. Schematic current patterns corresponding (a) to Fig. 7(i) and (b) to Fig. 7(j).

If the field is rotated counterclockwise after its initial application, a different set of current lines (and other characteristic patterns) nucleates with mirror symmetry to structures appearing in the cw rotation, as shown in Figs. 7(k) and 7(l) (see also Ref. 12). Note that if the in-plane field rotation is cw for the top face of the plate, it is ccw looking from the bottom face. Thus, observations on the top face with a given field rotation direction reproduce the picture on the bottom side with the opposite direction of rotation. From comparison of Figs. 7(k) and 7(l) it follows that at the bottom surface the current structures should run parallel to those on the top face. However, the directions of the currents are opposite on the two faces. It is likely that the ends of current lines on the two sides are connected through the thickness of the sample and form a closed current loop. In the case of the spiral ends of the pinches [as in Fig. 7(j)] the flow of the current from the ab surface into the bulk seems to be the only possible explanation for the apparent disappearance of the current line.

Patterns similar to those discussed above were observed on the ab faces of all YBCO crystals studied. They show that, in a superconducting plate in a rotating in-plane field, a highly inhomogeneous three-dimensional flux and current structure is formed. Details of the structure depend on the history of previous rotations, on the angle of rotation, the temperature and field, and the rotation speed. In samples with irregular shape and those with defects, the Meissner hole patterns are not symmetric. The effect of the external field in stabilizing the Meissner hole against bending can be seen by comparison of the unidirectional and rotated field patterns. In unidirectional fields [Fig. 3(d), see also pictures in Ref. 1], where the external field is perpendicular to the Meissner hole, it bends severely, while in the rotated field [Figs. 7(d)–7(f)], where the external field is more nearly aligned with Meissner hole, it is smooth.

B. Quantitative features of flux patterns in rotating fields

Quantitative characteristics of the above flux structures can be obtained from profiles of the normal component of induction along chosen directions on the sample surface. Such $B_n(x)$ curves measured along horizontal tracks in the center of the sample are shown in Figs. 10(a) and 10(b) for images in Figs. 7(a) and 7(f), respectively. One can see that the normal field at the edges (marked by arrows) and around the Meissner holes [marked by circles in Fig. 10(b)] is rather large (~ 150 G) even with a strong in-plane field (~ 1 kOe). The concentration of B_n at the sample edges is natural for plates with a circulating shielding current. The normal field drops very sharply from the edges just inside the crystal that indicates the dominant contribution of Meissner currents J_M flowing in the thin layer on the end face. A fit of the profile in Fig. 10(a) is shown by the dashed curve. The calculation was made for an infinitely long plate with the same cross section as the sample carrying $\pm J_c(\sim 1.2\times 10^5$ A/cm$^2)$ in the upper and lower halves and $\pm J_M(\sim 9\times 10^6$ A/cm$^2)$ in λ layers at the end faces as shown in the inset.

The strong normal field around the Meissner holes in Fig. 10(b) implies substantial current flowing along them. This effective current should have two contributions: a positive one, due to the Meissner current along the boundary of the flux-free cylinder, and a negative one, due to the absence of the critical current inside it. Relative to the surrounding bulk, the total current associated with the Meissner hole will be $I_{MH}\sim J_M 2\pi R_c\lambda - \pi R_c^2 J_c$. Here the first term corresponds to the boundary between Meissner and vortex phases that carries a magnetization current density $J_M\sim(1/\mu_0)B_{c1}/\lambda$ in the λ layer[5] and the second term accounts for the absence of J_c inside the cylinder. In an isotropic superconductor the line tension σ equals the vortex line energy $\varepsilon = B_{c1}\Phi_0/\mu_0$, so

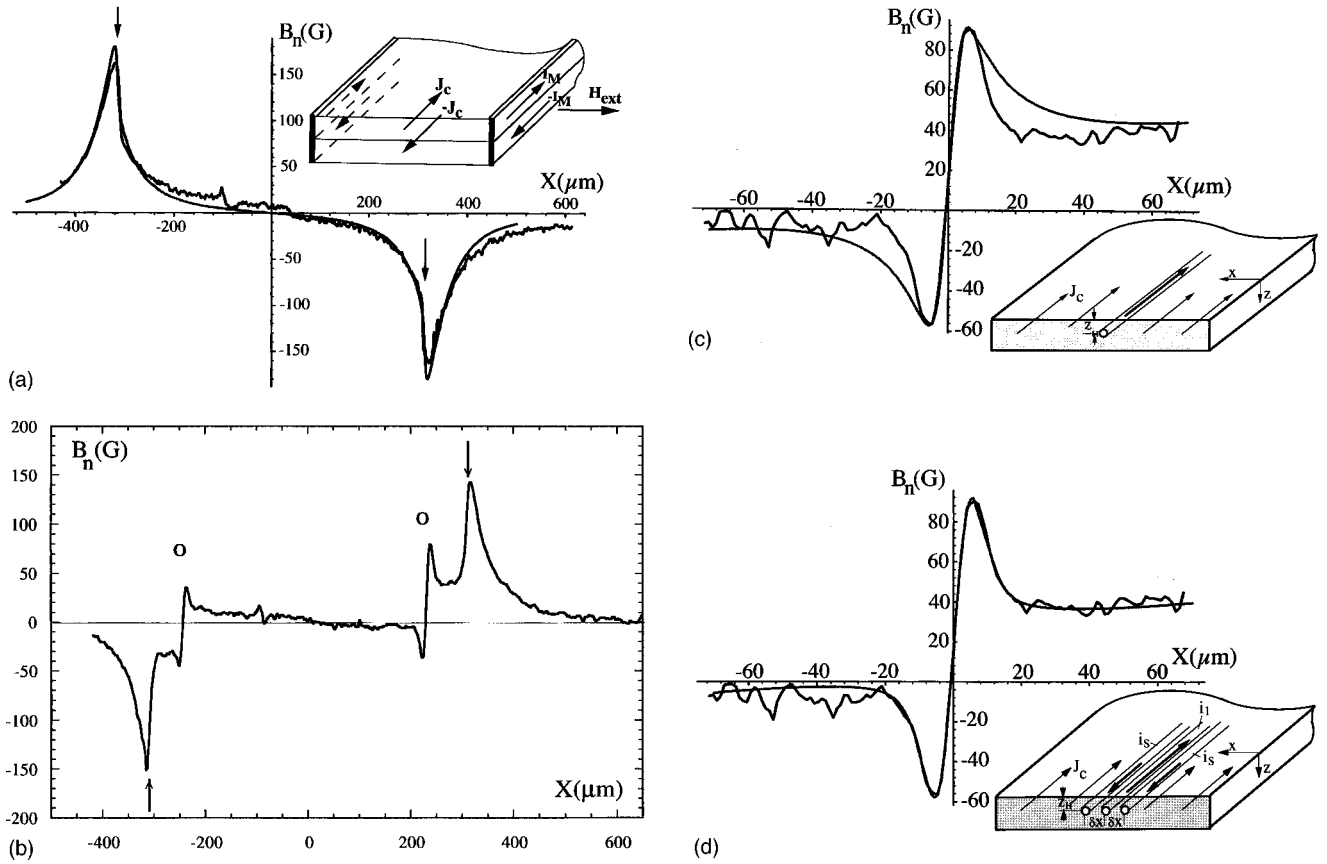

FIG. 10. Horizontal $Bn(x)$ scans across the ab face of the sample shown in Fig. 7. (a) application of the field [Fig. 7(a)], (b) rotation of H by 90° [Fig. 7(f)], (c,d) scans perpendicular to the right bright line in Fig. 7(f) with different fitting curves. Insets show current models used for fitting the experimental field profiles.

$R_c = B_{c1}/\mu_0 J_c$ and $I_{MH} \sim \pi (B_{c1}/\mu_0)^2 / J_c$. Note that the loss of the critical current in this case is exactly half of the gain in the Meissner current. Thus, Meissner holes produce a net increase of the local current. For regions outside the Meissner hole ($R > R_c$), the field of the excess current is identical to that for a line along the flux-free cylinder axis carrying the same current: $B_{MH} = \mu_0 I_{MH}/2\pi R$. Then the normal field at the sample surface is $B_n(x) = (\mu_0 I_{MH}/2\pi) x/(z_H^2 + x^2)$ if the hole axis is at a distance $z_H > R_c$ below the surface. This normal field distribution has extrema at $x = \pm z_H$ on either side of the hole, with amplitude $\mu_0 I_{MH}/(4\pi z_H)$.

The above picture of Meissner holes as developed in Refs. 3 and 4 for isotropic superconductors, and used also in Ref. 10 to explain changes in the $B_n(x)$ slope at the remagnetization front in BSCCO, qualitatively describes the observed features of images illustrated in Figs. 3, 5, and 7. However, as shown recently,[1] this simple model must be essentially modified in the case of anisotropic materials.

Anisotropy distorts the circular shape of Meissner holes because both the line tension and pinning, which determine the local radius, depend on the orientation of the vortex. These two anisotropies drive the Meissner hole shape in opposite directions. The line tension is lowest for vortex orientations in the ab plane and thus stretches the loops horizontally. In contrast, pinning is smallest for c-oriented vortices and favors horizontal contraction of the loops.

Although it is difficult to calculate the shape of the vortex loop minimizing its total energy in the presence of pinning anisotropy, it is possible to estimate the appropriate c and ab radii of the curvature of the loop. The knowledge of these radii is sufficient to define an ellipse that approximates the shape of the Meissner hole. In an anisotropic superconductor the line tension is[22]

$$\sigma_\theta = \varepsilon(\theta) + \partial^2 \varepsilon / \partial \theta^2 .$$

Taking $\varepsilon(\theta) = \varepsilon_0 k_\theta \ln(\lambda/k_\theta \xi)$, with $\varepsilon_0 = \Phi_0^2/4\pi\mu_0\lambda^2$ and $k_\theta = (\kappa^2 \cos^2\theta + \sin^2\theta)^{1/2}$ (Ref. 23) (here an anisotropy coefficient for YBCO $\kappa \sim \frac{1}{5} - \frac{1}{7}$, $\lambda/\xi \sim 50$, and θ is the angle between the vortex and the ab plane) one obtains

$$\sigma_\theta = \varepsilon_0 [(\kappa^2/k_\theta^3) \ln(\lambda/k_\theta \xi) - (1-\kappa^2) k_\theta^{-1} \cos 2\theta].$$

For vortex segments along the ab plane ($\theta = 0$) the line tension will be $\sigma_{ab} = (\varepsilon_0/\kappa)[\ln(\lambda/\kappa\xi) - 1 + \kappa^2]$ and for those along the c axis ($\theta = \pi/2$) $\sigma_c = \varepsilon_0\{1 + \kappa^2[\ln(\lambda/\xi) - 1]\}$. Accounting also for the ratio of pinning forces for the ab and c-vortex segments, $\mathscr{k}_p = F_{p,ab}/F_{p,c} \sim 3-4$ for YBCO crystals,[24] one gets an estimation for ratio of the curvature radii ($R_i \sim \sigma_i/F_i$) of the top and bottom loop segments (close to the ab plane) to those of left and right segments ($\sim$along the c axis): $R_{ab}/R_c \sim (\sigma_{ab}/\sigma_c)/\mathscr{k}_p \sim 5.1$ (for $\kappa = \frac{1}{5}$, $\mathscr{k}_p = 4$)–10.7 (for $\kappa = \frac{1}{7}$, $\mathscr{k}_p = 3$). Below, all estimates will be presented in couples for these two sets of κ and $\mathscr{k}_p$ to show that the possible range of estimated parameters is not wide.

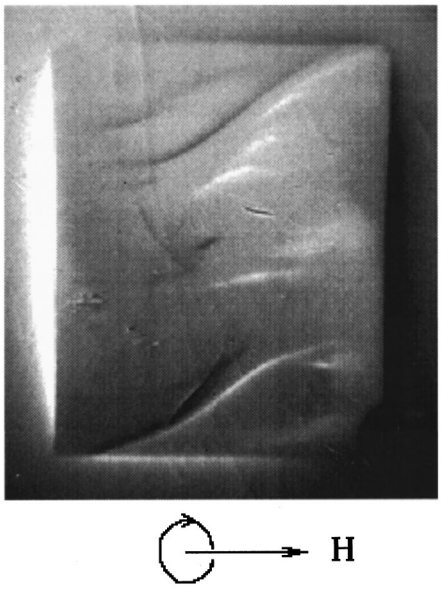

FIG. 11. Splitting of the Meissner hole images. The field was decreased from 970 to 490 G after rotation by 360°. $T=40$ K.

From the values of R_i it is easy to get the semimajor and semiminor axes a and b [for the ellipse $(x/a)^2+(z/b)^2=1$] using the known relation between the ellipse parameters $a=(R_{ab}^2R_c)^{1/3}=(2.96-4.86)R_c$ and $b=(R_{ab}R_c^2)^{1/3}=(1.72-2.2)R_c$. Note that the ratio of the ellipse semiaxes $a/b=(R_{ab}/R_c)^{1/3}$ is only ~ 2. The effective ellipticity of the Meissner hole is expected to be even smaller due to increased critical currents near its top and bottom, as shown below. This is consistent with observations of the Meissner holes for $H\|c$ (Ref. 1) that revealed that the widths of the hole images on the basal plane and on the end faces of YBCO crystals are very close. In this case, minimum widths were compared because, as mentioned above, they correspond to Meissner holes near the surface where actual and imaged dimensions are closest.

A strong increase of the ellipticity of Meissner holes was observed when the field was decreased after rotation. In this case the image of the Meissner holes splits, as shown in Fig. 11, corresponding to a flattening of the Meissner holes. This is associated with the expansion of vortex loops forming the Meissner hole in decreasing field.

An estimate of the magnetization current along the surface of an elliptic Meissner hole in an anisotropic material gives

$$I_M\sim(\pi/\mu_0)(R_{ab}B_{c1}^{ab}+R_cB_{c1}^c)\sim(\pi/\mu_0)(2-2.53)R_cB_{c1}^c \sim(0.7-0.85)\text{A}.$$

Here the ellipse is approximated by two arcs with the radius R_c and two arcs with R_{ab} and with currents across them (i.e., along the cylinder surface) having the linear density B_{c1}^c/μ_0 and $B_{c1}^{ab}/\mu_0=\kappa B_{c1}^c/\mu_0$, respectively. Note that the length of the ab segments is larger, but their contribution to I_M is the same as for the c segments due to smaller B_{c1}^{ab}. An alternative but close estimate, $I_M\sim(\pi/\mu_0)(2.14-2.78)R_cB_{c1}^c \sim(0.75-0.93)$A is obtained by taking the more exact expression for the ellipse length $L\approx\pi[1.5(R_{ab}R_c)^{1/3}(R_{ab}^{1/3}+R_c^{1/3})-(R_{ab}R_c)^{1/2}]\sim\pi(4.76-7.32)R_c$ and an average Meissner current $(1/\mu_0)(B_{c1}^{ab}B_{c1}^c)^{1/2}\sim(1/\mu_0)(0.45-0.38)B_{c1}^c$.

Taking ε_0 in the form $\varepsilon_0=(\Phi_0B_{c1}^c)/\mu_0\ln(\lambda/\xi)$ and $R_c=\sigma_c/\Phi_0J_c^c$ (with $B_{c1}^c\sim 280$ G and $J_c^c\sim 1.28\times10^5$ A/cm^2 obtained from fits of the induction profiles in the c-oriented field),[1] one gets $R_c\sim 5\,\mu$m. Due to the large $R_{ab}\sim(5-10)R_c$, the cross-sectional area of the cylinder $S=\pi R_{ab}R_c$ is large and thus the losses in the critical current inside the hole will be large: $\Delta I_c=SJ_c^{av}\sim(1.28-1.95)$A, with $J_c^{av}\sim 0.5(J_c^{ab}+J_c^c)$. The loss of J_c inside the Meissner hole is now about two times larger than the Meissner current I_M along the cylinder surface. In the images this would correspond to an inverted contrast on the Meissner holes as compared to that observed in the experiment.

To explain the observed polarity and values of the fields around the Meissner hole, one has to account for anisotropic critical currents surrounding the flux-free cylinder. In our geometry on the top and bottom of the hole, vortices are primarily oriented along the ab direction and the critical current density is larger than on the right and left of the hole where the vortices are oriented primarily along c. This excess critical current above and below the hole and the reduced critical current to the left and right distort the field symmetry and give a sufficient net contribution to the apparent total current along the Meissner hole.

To model $B_n(x)$ above the Meissner hole, we simulated the latter by three current lines at a distance z_H from the surface immersed in a current carrying a bar of rectangular shape. The central line with a current i_1 represents the Meissner current on the surface of the cylinder, the loss of critical current inside it, and the excess current above and below the hole. Two satellites with negative currents i_s correspond to reduced currents adjacent to the hole. Figures 10(c) and 10(d) show both one and three wire fits of the profile measured perpendicular to the Meissner hole on the right in Fig. 7(e). In the fits, currents distant from the Meissner hole were assumed to be constant. For the single wire model the fit in Fig. 10(c) gives the current in the wire $i=0.4$ A and its position at 6 μm below the surface. The single wire model for the Meissner hole does not allow the sharp wings of the experimental $B_n(x)$ to be fitted. For the three wire fit [Fig. 10(d)] the central current is $i_1=+1.22$ A at 9.4 μm below the surface and satellites $i_s=-0.49$ A are at 6.5 μm on both sides of i_1. A background current $J=1.35\times10^5$ A/cm^2 for both fits accounts for the variation of $B_n(x)$ at a larger distance from the Meissner hole. i_1 is a sum of the current due to the Meissner cylinder (surface current minus loss of J_c inside it) $I_{MH}=I_M-\Delta I_c$ and the positive contribution δI^{ab} due to the larger J_c at the top and bottom of the Meissner hole. Using the earlier estimates $I_M\sim(0.7-0.85)$A and $\Delta I_c\sim(1.28-1.95)$A, the fit value of i_1 implies that $\delta I^{ab}\sim+(1.8-2.3)$A. These estimates of δI^{ab} and i_s show that the anisotropic critical currents around the flux-free cylinder give major contributions to the total current associated with the Meissner hole and reduce the anisotropy of its field profile.

If the closed vortex loops around the Meissner hole are entangled,[25] the critical current near the hole may be en-

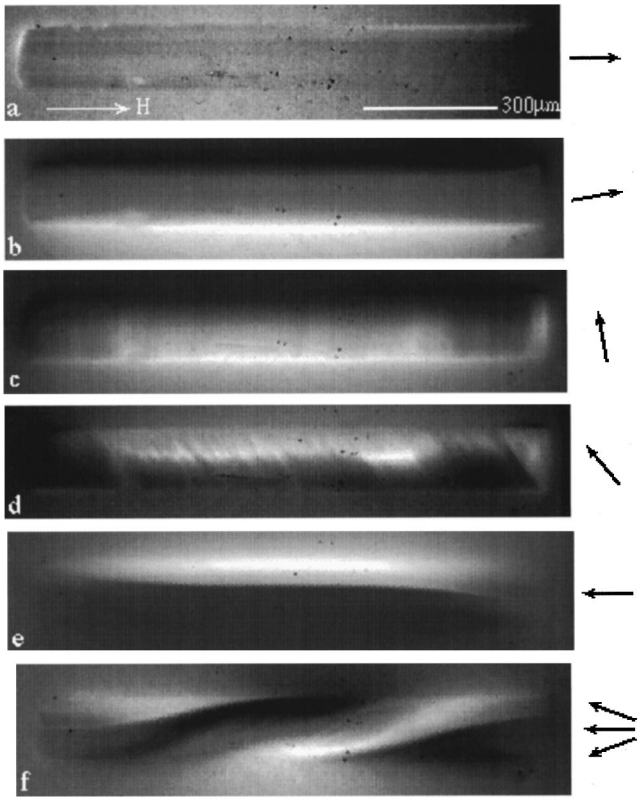

FIG. 12. Rotation of the field in the end face plane at $T=50$ K. $H=1250$ Oe is applied along the horizontal direction and rotated as shown by the arrows. At $\alpha\sim180°$ (e) a horizontal line of increased contrast is formed in the middle of the face. In (f) the field was turned several times by $\sim\pm20°$ around 180° and the contrast split into two parts. Note a qualitative similarity between Figs. 12(f) and 7(f).

hanced. This larger J_c would reduce the critical radius and shrink the Meissner hole. A qualitatively similar increase of pinning near the Meissner hole can arise from the field dependence of J_c, which should increase as B goes to 0.

V. OBSERVATIONS IN THE FIELD ROTATED IN THE END FACE PLANE

In the end face experiments crystals were turned with one of their ac or bc surfaces perpendicular to the microscope optic axis and the field was rotated in the plane of this face, as illustrated in Fig. 2(d). Pictures of flux distributions on the end faces of the samples showed a qualitative similarity to images observed on the ab surfaces in rotated fields.

When the field was initially applied parallel to the long side, only positive (bright contrast) and negative (dark contrast) stray normal fields at the right and left short edges were observed [Fig. 12(a)]. With rotation of the field, strong normal fields of opposite polarities appeared also at long edges [Fig. 12(b)] and entered deeper in the sample with increasing angle. The image in Fig. 12(b) is reminiscent of the picture observed on the end face for a unidirectional field along the c axis [see Fig. 5(a)]. This resemblance is due to the dominating effect of the ab currents that effectively screen the c component of the external field in Fig. 12(b).

With further field rotation, stripes along the c axis are revealed, which are associated with modulations of induction due to twin domains crossing the end face [Fig. 12(c)]. When the field passes the normal to the long side (i.e., the normal to the ab plane) brighter stripes oriented close to the field direction appear [Fig. 12(d)]. They are developed at fields turned from the initial direction by $\alpha\sim120$ to 170°. The stripes correspond to modulations of the normal field components on the end face and are similar to modulated structures observed near the edges on the ab face after field rotation in the ab plane [see Figs. 7(c) and 7(d)]. They can be associated with the helical instability due to crossing of entering and trapped flux lines as discussed in Sec. IV A. At $\alpha\sim180°$, the stripes disappear and a bright contrast develops on the long edges ~parallel to the field [Fig. 12(e)]. The contrast in Fig. 12(e) is inverted with respect to Fig. 12(b). It corresponds to inversion of the normal components of induction on the top and bottom sides of the sample that arises from the c component of the flux trapped during rotation of the field. Qualitatively, the effect is the same as illustrated in Figs. 3(a) and 3(b) and discussed in Sec. III A.

An important feature in Fig. 12(e) is a horizontal line with local, large and opposite B_n components adjacent to it. As was shown in Fig. 5, a similar structure is formed when the sample is remagnetized by a unidirectional field normal to the basal plane. However, in the latter case the boundary is usually bending and regions of increased B_n localized inside the strong bends move along it. In both situations, when the field component perpendicular to the ab plane decreases, flux lines trapped in a strong perpendicular field close into loops at the end face, resulting in formation of the Meissner hole (as in Fig. 6). In the case of the unidirectional c field, excess current in the Meissner hole is subject to the bending instability. In the field rotating in the end face, the Meissner hole is stabilized by the external field parallel to the long edge and is straight. However, if the external field is rotated back and forth near the angle of 180°, the Meissner hole can be split into two parts and a picture topologically similar to that observed on the ab plane in rotating field is obtained [compare Figs. 12(f) and 7(f)].

The formation of lines of excess current showing the same contrast as Meissner holes was also observed in YBCO crystals subject to an ac field along the c axis in the presence of a dc field in the ab plane.[26] It is reminiscent of the successive formation of Meissner holes near the sample edges when the c-directed ac field only is applied.[1] However, in the latter case Meissner holes are not straight but strongly wiggle and form domains of vortices of opposite polarities. These regions slowly drift in the ac field to the interior of the sample, forming a specific dynamic domain structure in superconducting plates.[1]

VI. CONCLUSION

The experimental observations presented here show that, independently of the sample geometry and the field orientation in any finite superconductor, the remagnetization by unidirectional and rotating fields proceeds not by escape and entry of approximately straight vortex segments but by bending of vortices and shrinking of closed flux lines. There are always conditions during the remagnetization cycle when vortices close into small loops that then collapse and form

flux-free Meissner holes. The excess local current along the Meissner holes can be large and increase the field and vortex density nearby. In high-T_c superconductors the dominating contribution to this current is the anisotropic critical currents in the near environment of the Meissner hole. Excess currents around the Meissner hole can also occur in isotropic superconductors if the field dependence of J_c is strong enough. In this case the isotropic critical currents are largest near the Meissner hole where the field is smallest. Formation of Meissner holes is observed even in fields parallel to the plane of thin plates.

An important consequence of the appearance of the excess current along Meissner holes is the generation of macroscopic flux instabilities. They show themselves through bending and decaying of the current lines into mobile macroscopic current loops enclosing flux bundles. Such a specific dynamic domain structure is an intrinsic feature of remagnetized superconductors.

ACKNOWLEDGMENTS

The work was supported by the U.S. DOE, BES-Materials Science (U.W., G.W.C.) under Contract No. W-31-109-ENG-38, the Russian National Program for High-T_c Superconductivity (Project No. 96056), and the NSF Science and Technology Center for Superconductivity (DMG) under Contract No. (DMR91-20000).

[1] V. K. Vlasko-Vlasov, U. Welp, G. W. Crabtree, D. Gunter, V. Kabanov, and V. I. Nikitenko, Phys. Rev. B **56**, 5622 (1997).
[2] A. M. Campbell and J. E. Evetts, *Critical Currents in Superconductors* (Taylor & Francis, London, 1972).
[3] H. Koppe, Phys. Status Solidi **17**, K229 (1966).
[4] J. E. Evetts and A. M. Campbell, in *Proceedings of the Xth International Conference on Low Temperature Physics*, edited by M. P. Malkov (VINITI, Moscow, 1967), Vol. II B, p. 33.
[5] H. Ullmaier, *Irreversible Properties of Type-II Superconductors* (Springer, New York, 1975).
[6] J. Clem, J. Appl. Phys. **50**, 3518 (1979).
[7] Y. Yeshurun, A. P. Malozemoff, and F. Holtzberg, Phys. Rev. B **38**, 11 828 (1988).
[8] L. Krusin-Elbaum, A. P. Malozemoff, D. C. Cronmeier, F. Holtzberg, J. R. Clem, and Z. Hao, J. Appl. Phys. **67**, 4670 (1990).
[9] M. A. R. LeBlanc, S. X. Wang, D. LeBlanc, M. Krzywinski, and J. Meng, Phys. Rev. B **52**, 12 895 (1995).
[10] M. V. Indenbom, Th. Schuster, H. Kuhn, H. Kronmuller, T. W. Li, and A. A. Menovsky, Phys. Rev. B **51**, 15 484 (1995).
[11] V. K. Vlasko-Vlasov, V. I. Nikitenko, A. A. Polyanskii, G. W. Crabtree, U. Welp, and B. W. Veal, Physica C **222**, 361 (1994).
[12] V. Vlasko-Vlasov, U. Welp, V. Kabanov, G. Crabtree, and V. Nikitenko, Pis'ma Zh. Eksp. Teor. Fiz. **65**, 253 (1997) [JETP Lett. **65**, 264 (1997)].
[13] L. A. Dorosinskii, M. V. Indenbom, V. I. Nikitenko, Yu. A. Ossipian, A. A. Polyanskii, and V. K. Vlasko-Vlasov, Physica C **203**, 149 (1992).
[14] A. Yu. Martinovich, Pis'ma Zh. Eksp. Teor. Fiz. **57**, 478 (1993) [JETP Lett. **57**, 497 (1993)].
[15] J. R. Reitz, F. J. Milford, and R. W. Christy, *Foundations of Electromagnetic Theory* (Addison-Welsley, Reading, MA, 1993), p. 353.
[16] J. R. Clem, Phys. Rev. Lett. **24**, 1425 (1977).
[17] E. H. Brandt, Phys. Lett. **79A**, 207 (1980); J. Low Temp. Phys. **44**, 33 (1981).
[18] D. G. Walmsley, J. Phys. F **2**, 510 (1972).
[19] J. R. Clem and A. Perez-Gonzalez, Phys. Rev. B **30**, 5041 (1984); A. Perez-Gonzalez and J. R. Clem, *ibid.* **31**, 7048 (1985).
[20] M. K. Hasan and J. S. Kouvel, Physica C **276**, 289 (1997).
[21] R. Boyer and M. A. R. LeBlanc, Solid State Commun. **24**, 261 (1977); R. Boyer, G. Fillon, and M. A. R. LeBlanc, J. Appl. Phys. **51**, 1692 (1980); J. R. Cave and M. A. R. LeBlanc, *ibid.* **53**, 1631 (1982).
[22] A. Sudbo, E. H. Brandt, and D. A. Huse, Phys. Rev. Lett. **71**, 1451 (1993).
[23] G. Blatter, M. V. Feigel'man, V. B. Geshkenbein, A. I. Larkin, and V. M. Vinokur, Rev. Mod. Phys. **66**, 1125 (1994).
[24] D. Lacey, L. F. Cohen, G. K. Perkins, J. S. Abell, and A. D. Caplin, Physica C **235–240**, 2595 (1994).
[25] D. Ertas and D. R. Nelson, Physica C **272**, 79 (1996).
[26] M. V. Indenbom, C. J. van der Beek, V. Berseth, W. Benoit, G. D'Anna, A. Erb, E. Walker, and R. Flukiger, Nature (London) **385**, 702 (1997).